Pol. J. Environ. Stud. Vol. XX, No. X (XXXX), 1-15
DOI: *10.15244/pjoes/216174* ONLINE PUBLICATION DATE: 2026-05-14

Original Research

Numerical Simulation and Prediction Study of Surface Subsidence Induced by Underground Mining at Pulang Copper Mine

Xinglong Feng[1], Xining Sun[2], Liang Li[1], Zhongwei Fu[2], Mingchuan Hu[1], Huiyun Wang[2], Zihao Leng[3], Guangyin Lu[3]°*

[1]Yunnan Diqing Nonferrous Metal Co., Ltd., Shangri-La 674400, Yunnan, China
[2]China Nonferrous Metal Industry Kunming Exploration and Design Research Institute Co., Ltd, Shangri-La 674400, Yunnan, China
[3]School of Geosciences and Info-physics, Central South University, Changsha 410083, Hunan, China

Received: 15 August 2025
Accepted: 29 December 2025

Abstract

Ground subsidence and surface collapse induced by underground mining have long been central concerns in rock mechanics and mining engineering. Such failures disrupt stratigraphic integrity and pose severe threats to local ecosystems and the lives and property of mine personnel. This study, focusing on the Pulang Copper Mine in Yunnan Province, employs a three-dimensional numerical modelling approach to investigate surface deformation resulting from block-caving operations. A high-resolution 3D geological model was constructed to elucidate the mechanisms driving ground movement, particularly emphasising the collapse evolution above the southern mining district following extraction in the initial caving panel. Simulation results indicate that continued mining in the district's south progressively enlarges the overlying subsidence basin. Comparison of simulated displacements and collapse extents with field measurements confirms the reliability of the calibrated model. Based on this, we forecast potential surface collapse zones associated with future mining schedules, providing quantitative guidance for mine safety management and environmental protection.

Keywords: subsidence, numerical simulation, collapse prediction

Introduction

Research Background

With ever-increasing global demand for mineral resources, mining has generated substantial economic benefits while inevitably giving rise to safety and environmental challenges. Among these, surface subsidence and collapse induced by underground extraction are among the most common and severe geohazards in mining districts, as they damage surface infrastructure, degrade ecosystems, and significantly constrain the sustainable development of mines.

Systematic research on mining-induced subsidence can be traced back to the mid-nineteenth century,

*e-mail: 127293@csu.edu.cn
°ORCID iD: 0000-0002-8014-819X

when Belgian engineer Gonot proposed the vertical curve theory, one of the earliest mathematical models to quantify the extent of mining subsidence. Since then, numerous scholars have advanced the theoretical understanding of ground deformation. Blodgett et al. [1] reviewed cases of underground hard-rock metal mines in the United States and elsewhere, evaluating resultant subsidence, environmental effects, and hydrological impacts while offering mitigation strategies. Luo et al. [2] improved prediction accuracy by modifying the Knothe influence function; Huayang et al. [3] employed the integral probability method to elucidate the deformation mechanism of subsidence beneath thick loess layers; Wan et al. [4] developed a dynamic subsidence model based on the Knothe time function for coal mines; Yan et al. [5] proposed a log-normal model for inclined subsidence, and Zhang et al. [6] further refined the Knothe time function to predict time-dependent settlement. Nasiri et al. [7] conducted a spatial analysis of the parameters affecting subsidence using the OLS model, while Li et al. [8] combined InSAR-derived time series with the FWBM model to assess ground-settlement hazards. Rosa et al. [9] introduced a GIS-based multi-criteria framework for urban mining-disaster assessment and mitigation.

Due to the high cost, time-consuming nature, and limitations in scale and parameter range of physical models, scholars have begun to deploy monitoring devices on the subsided surface to study subsidence impacts. On-site monitoring technology provides a direct and effective means for studying surface deformation and rock movement. The data obtained can accurately reflect surface displacement in mining areas, promptly guide mining activities, and support design. Guéguen et al. [10] used PSI and DInSAR to monitor subsidence in a 15-year-old mined-out area from 1992 to 2007. Zhao et al. [11] revealed the surface deformation lag response mechanism from different perspectives through monitoring results. Xia et al. [12] employed ultra-deep multipoint extensometers to investigate the mechanism of deep rock mass movement. Gong et al. [13] monitored subsidence using traditional GPS and leveling methods in the North China Plain. Wempen et al. [14] used DInSAR to monitor surface subsidence. Ma et al. [15] developed a three-dimensional testing device to simulate the impact of coal mining on rock strata movement. Peng et al. [16] combined multi-temporal InSAR and ICA methods to study surface deformation in groundwater basins. Muhetaer et al. [17] analysed the evolution pattern of Beijing's ground subsidence based on PS-InSAR technology. Ma et al. [18] applied SBAS-InSAR technology, object-oriented classification, and normalized difference vegetation index, combined with summer precipitation data, to analyse the relationship between ground subsidence, subsidence-induced water, and vegetation changes.

In recent years, with the emergence of high-capacity, high-speed computers, numerical analysis methods have been widely applied to simulate the movement of underground rock strata and surface deformation. Thanks to continuous innovation and advances in computer technology, high-precision modelling and detailed numerical analysis of complex geological structures are now possible, significantly improving the accuracy and reliability of mining subsidence predictions. Mancini et al. [19] assessed the subsidence phenomena in underground salt mines using data provided by GPS measurements, pressure records, and curvature analysis. Helm et al. [20] studied the impact of groundwater level changes on abandoned mines using FLAC^{3D} parametric modelling. Huang et al. [21] discussed the estimation of surface subsidence caused by mining and backfilling at the Luohe mine using DEM modelling. Salmi et al. [22] employed DEM to study the mechanisms of slope instability induced by mining at Nattai North. Hamdi et al. [23] used finite/discrete element modelling to investigate the impact of discontinuity, persistence, and spacing on surface subsidence. Wu et al. [24] investigated the effect of geological parameters on CSG mining subsidence using numerical methods. Liu et al. [25] simulated the development of face subsidence using 3DEC numerical software. Chen et al. [26] validated the mining deformation mechanism by comparing SBAS-InSAR and leveling measurement data. Parmar et al. [27] simulated surface subsidence caused by the sub-layer collapse method using FLAC^{3D} software. Zhao et al. [28] constructed a 3D model using FLAC^{3D} to assess the stability of shafts and surface deformation resulting from underground mining transfer in open-pit mining. Cai et al. [29] proposed an integrated prediction method based on the InSAR-FLAC^{3D} probabilistic integral method to predict surface deformation caused by mining thin coal seams. Zhou et al. [30] combined numerical simulation and SBAS-InSAR to study the subsidence patterns induced by multiple coal seam mining. Gong et al. [31] proposed the Data Intensive Modeling Method (DINMM) and validated its prediction accuracy. Among these, FLAC^{3D} software is recognized for its excellent stability and efficiency, making it more suitable for the numerical simulation of large deformations in mined-out areas than other software.

Collectively, these developments underscore the transition from purely empirical or observational studies to sophisticated, data-rich numerical analyses, facilitating more reliable assessment and mitigation of mining-induced ground deformation.

Engineering Background

The Pulang Copper Mine is in north-western Yunnan Province, within Shangri-La County of the Diqing Tibetan Autonomous Prefecture. It lies at the transitional boundary between the Tibetan Plateau's south-eastern rim and the Hengduan Mountains' north-eastern segment, adjacent to the "Three Parallel Rivers" World Natural Heritage Site. The deposit is situated in a remote, densely forested alpine region with pronounced topographic relief, where elevation ranges

from 3,450 m at the valley floor to 4,702 m at the highest peak. Geologically, the area is relatively homogeneous, dominated by massive, hard-rock lithologies, though localized fault zones are present.

Mining is conducted by the block-caving method. The operation begins with excavating an undercut at the base of the orebody, disrupting the initial stress equilibrium. Systematically arranged drawbells progressively enlarge the undercut span, inducing tensile fracturing in the overlying rock mass. As the extraction front advances, these fractures propagate and coalesce, ultimately leading to the large-scale caving of the ore under gravitational loading. The broken ore is withdrawn through a bottom draw-point system, while the cave propagates upward to form an extensive caved zone. Although block caving substantially reduces mining costs and gains in productivity, it inevitably generates significant surface subsidence. The underlying mechanism involves the loss of support in the caved void, the bending and sagging of overlying strata, and the upward propagation of deformation, culminating in the formation of a subsidence basin at the surface. A schematic representation of the collapse process is provided in Fig. 1.

Since mining commenced at the Pulang Copper Mine in 2017, progressive surface subsidence has developed above the initial production panel. By July 2023, this deformation had evolved into a surface collapse zone roughly 400 m in diameter, situated directly above the first mining area. The location of the subsidence pit is shown in Fig. 2.

Fig. 3 illustrates the underground mining zones and the corresponding surface collapse extent. The blue area denotes the initial mining panel, whereas the red outline

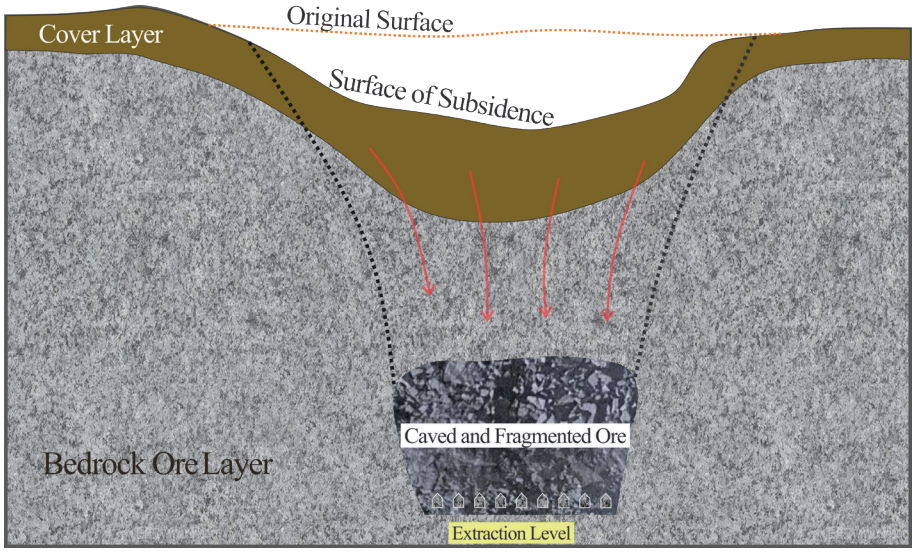

Fig. 1. Schematic diagram of surface subsidence caused by the block caving mining method.

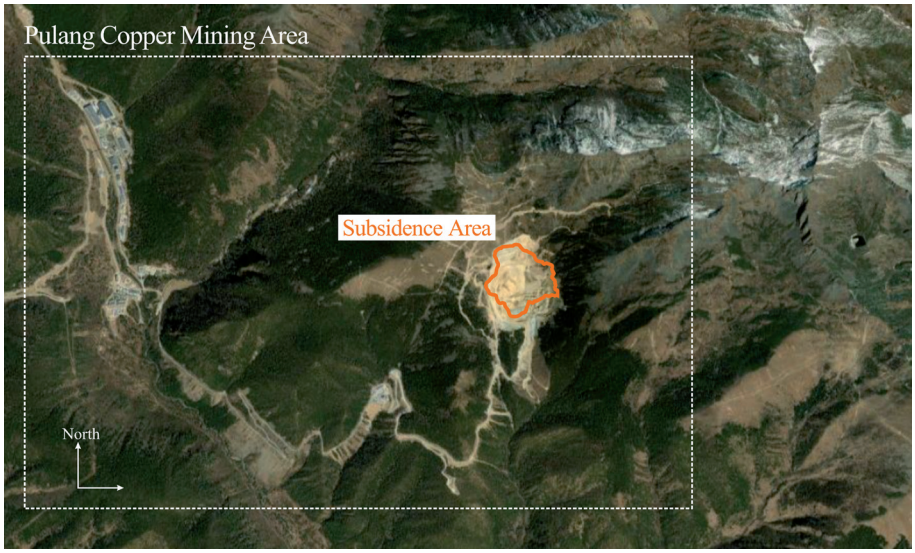

Fig. 2. Locations of the Mining Area and Subsidence Zone.

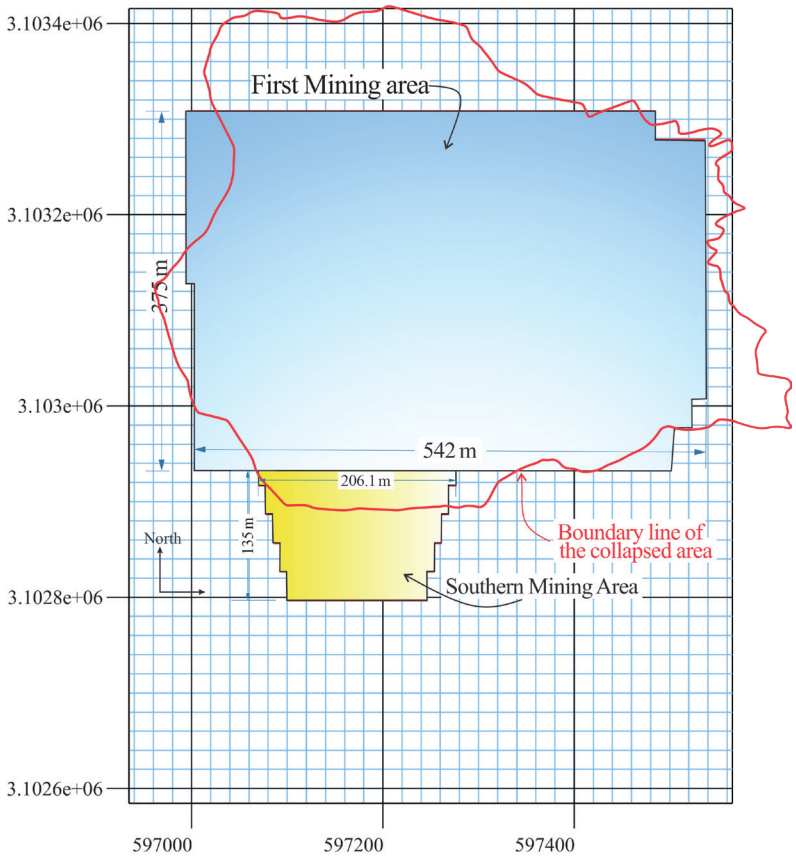

Fig. 3. Underground mining extent and initial subsidence boundary.

marks the boundary of surface subsidence induced by this panel as of July 2023. The yellow area south of the first panel represents the planned southern mining district.

Materials and Methods

Establishment of Three-Dimensional Geological Model

Based on the contour data of the surface subsidence zone surveyed in July 2023, a three-dimensional terrain model was generated in Rhino 7.0 and meshed in Griddle 2.0, and the resulting grid model was imported into FLAC^{3D} for subsequent numerical simulation. The model employs a fully hexahedral mesh with a uniform cell size of 4 m, comprising 3,705,872 elements and 2,862,390 nodes. The resulting 3D mesh is illustrated in Fig. 4.

The numerical model of the collapse zone is simplified into three components: an overburden layer, a subsidence (caved) zone, and intact bedrock. The coordinate system is defined with the X-axis pointing east and the Y-axis pointing north. Overall model dimensions are 821 m (East-West) by 1,420 m (North-South), with the model base set at 3,691 m. As illustrated in Fig. 5, the green volume represents the subsidence zone, with an average thickness of 60 m and a maximum of 180 m. The yellow volume denotes the overburden layer, averaging 16 m thick and locally thickening to 80 m. Progressive caving has caused continuous downward movement of the collapse zone, allowing large amounts of glacial till to infill the void. Because the exact thickness of the infilled till is uncertain, the model assumes a boundary elevation of 3,820 m to separate the overlying till from the underlying bedrock. The 3D model also incorporates the planned underground

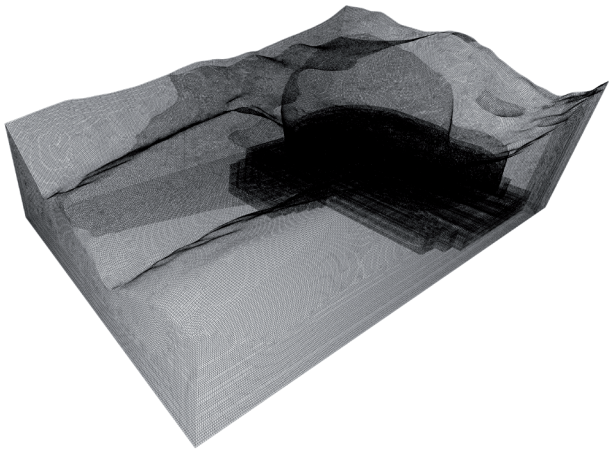

Fig. 4. 3D model grid.

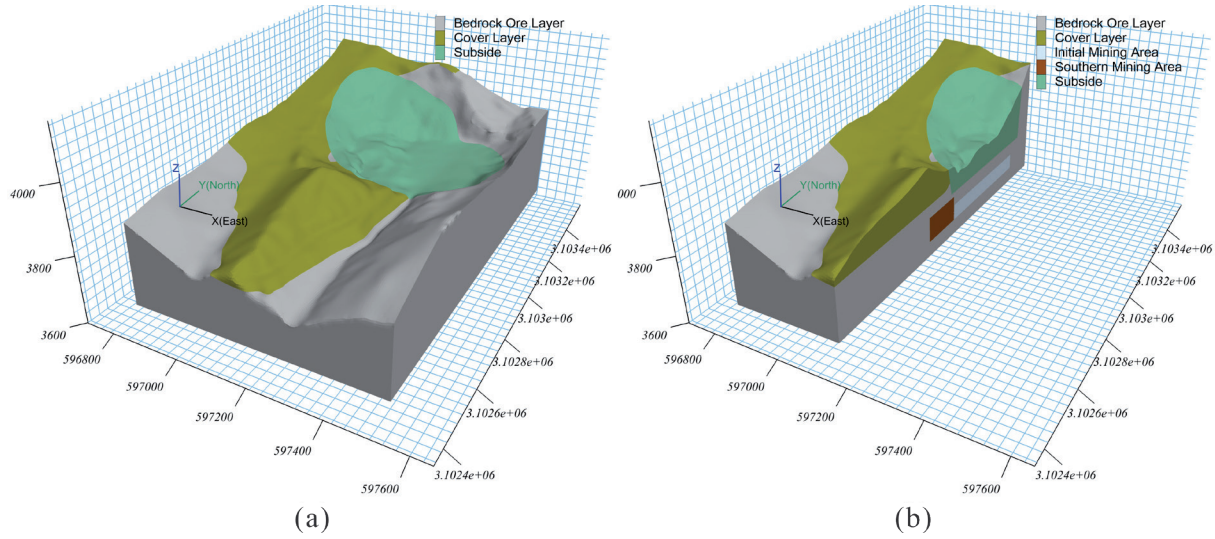

Fig. 5. a) Three-dimensional geologic model of the study area, b) Three-dimensional model section.

mining extents, as shown in the section view in Fig. 5b). The white volume beneath the collapse zone delineates the main orebody, while the brown volume to the south outlines the southern mining district.

Selection of Geomechanical Parameters

The study area is underlain chiefly by quartz monzonite porphyry, diorite porphyry, and marble. Because the orebody is hosted predominantly in the quartz monzonite porphyry, which also constitutes the bulk of the collapse zone, and the three rock types exhibit only minor differences in mechanical properties, the quartz monzonite porphyry parameters were adopted to represent the entire rock mass in the numerical model. Rock behaviour was simulated using the Mohr-Coulomb elasto-plastic constitutive model, which is widely employed in rock and soil mechanics to characterize the strength and post-yield response of granular geomaterials. The material obeys Hooke's law in the elastic range, whereas irreversible plastic deformation initiates once the stress state satisfies the Mohr-Coulomb yield criterion, as expressed in Eq. (1).

$$f_s = \sigma_1 - \sigma_3 \frac{1+\sin\varphi}{1-\sin\varphi} + 2c\sqrt{\frac{1+\sin\varphi}{1-\sin\varphi}} \tag{1}$$

σ_1 and σ_3 represent the maximum and minimum principal stresses, c and φ are the cohesion and internal friction angle.

Due to the influence of joint fractures, structural surfaces, and various complex environmental factors, the rock mechanics parameters measured in the laboratory often do not accurately represent the true in-situ properties of the rock mass. Therefore, it is necessary to apply a reduction factor to these parameters. The Hoek-Brown strength criterion, an empirical rock mass strength model widely used in geotechnical and mining engineering, is particularly suitable for predicting the strength of jointed or anisotropic rock masses. Proposed by E. Hoek and E. T. Brown in 1980, this criterion utilises the geological strength index (GSI) and uniaxial compressive strength of rocks to assess the nonlinear strength characteristics of the rock mass and subsequently adjust the laboratory parameters. The basic form of the criterion can be expressed as Eq. (2).

$$\sigma_1 = \sigma_3 + \sqrt{m_{\sigma_c}\sigma_3 + s\sigma_c^2} \tag{2}$$

σ_1 and σ_3 represent the maximum and minimum principal stresses acting on the rock specimen. c denotes the uniaxial compressive strength of the rock mass, while m and s are rock material constants.

The discounted parameters are shown in Table 1 below. In the table, ρ is the density, E is the modulus of elasticity, v is Poisson's ratio, c is the cohesion, σ is the strength resistance, and φ is the angle of internal friction.

Boundary Conditions and Numerical Simulation Approach

The model's top is a free surface in the numerical simulation. At the same time, usual displacement constraints are applied to the sidewalls, and displacement constraints in all three directions are imposed at the bottom. The calculation considers only the effect of gravitational stress on the rock mass. Given that the initial mining area has been fully excavated and surface subsidence is ongoing, a constant subsidence rate is applied to the roof of the mined central ore zone to simulate the collapse process and more accurately reflect the actual engineering conditions. After multiple parameter adjustments, a subsidence rate of 3×10^{-3} m/step is applied in the Z-direction. For the model with

Table 1. Geotechnical physical and mechanical parameters.

Parameters	Rock formation	Moraine cover layer	Subside
ρ / (kg/m^3)	2760	2100	2100
E / (GPa)	4.5	0.46	0.40
c / (MPa)	0.88	0.056	0.051
φ / (°)	27.8	34.9	32.1
v	0.25	0.11	0.1
σ / (MPa)	1.06	0.126	0.110

boundary conditions set, an excavation simulation of mining in the southern mining area is conducted to analyse displacement variation within the numerical model. A displacement monitoring line is also set within the model, positioned south of the mining area, as shown in Fig. 6. This monitoring line records the evolution of displacement characteristics of the overlying rock mass at various measurement points during the excavation process. The monitoring line is evenly spaced with 21 monitoring points. The spatial coordinates of monitoring point 1 are (597186, 3.10293×10^6, 3874.91), and the distance between adjacent monitoring points along the Y-direction is 10 m. The spatial coordinates of monitoring point 21 are (597186, 3.10273×10^6, 3874.91).

Results

Analysis of Numerical Simulation Results

The excavation simulation of the southern mining area was performed on the model in its initial state, with 4,000 steps conducted under gravitational stress. As shown in Fig. 7, the vertical displacement contour maps of the model cross-section are presented for four key stages: 1,000, 2,000, 3,000, and 4,000 steps.

The results shown in Fig. 7 indicate that, since the northern side of the southern mining area adjoins the initial mining area, the lateral confinement of the surrounding rock on this side is relatively weak. As a result, the overlying rock mass in this region is more susceptible to subsidence, exhibiting significantly greater vertical displacement compared to the southern side. As the simulation progresses, the cumulative displacement further accentuates the difference in displacement between the two sides. A comparison of the vertical displacement contour maps at each stage reveals that, although the magnitude of displacement changes significantly over time, the spatial extent of the affected area remains unchanged. This suggests that the boundary of surface subsidence stabilises before 1,000 steps, and subsequent modifications primarily manifest as increased displacement within the subsidence zone. After 4,000 simulation steps, the maximum vertical displacement of the stope roof exceeds 41 m, and the maximum surface vertical displacement reaches 39 m.

By comparing the surface displacement contour map in Fig. 8 with the underground mining extent

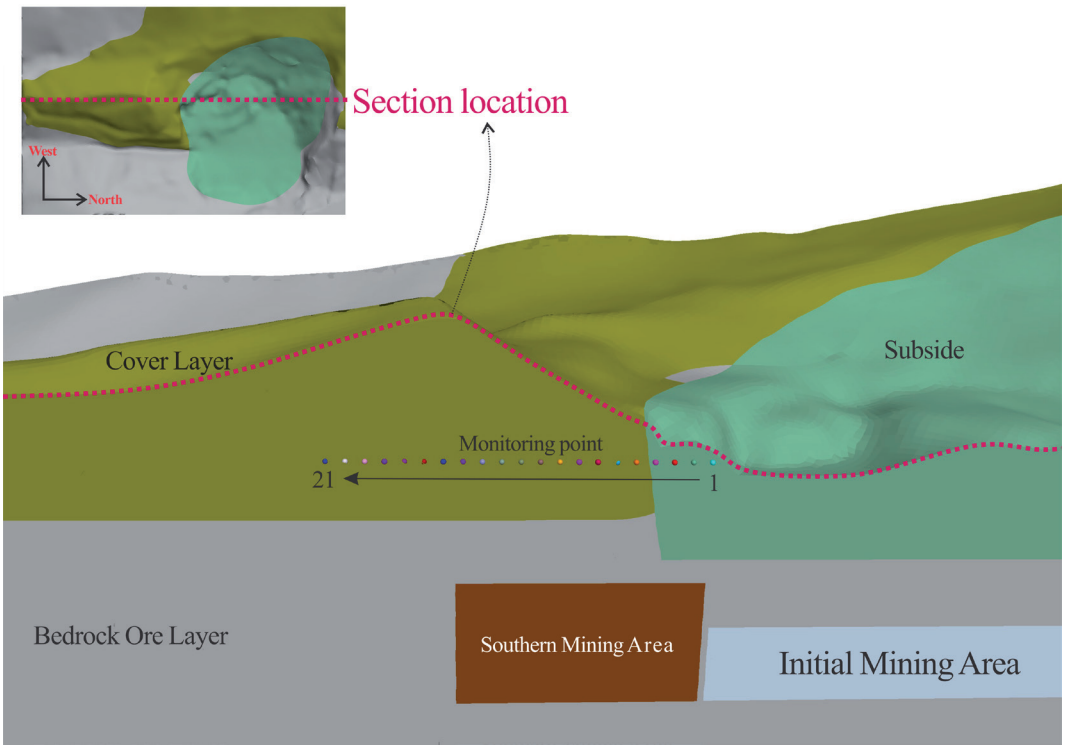

Fig. 6. Locations of monitoring points.

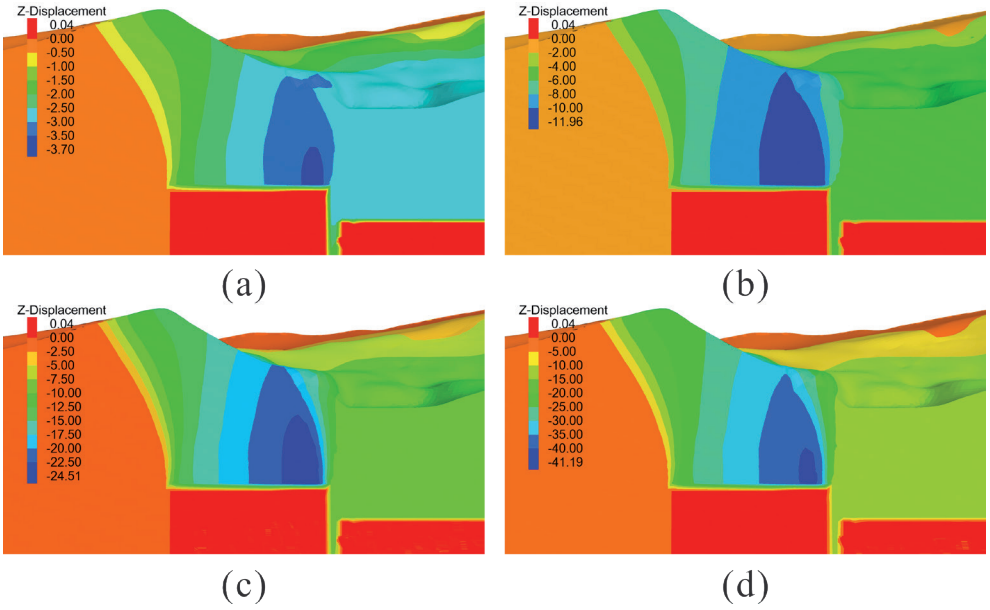

Fig. 7. The Z-direction displacement cloud map at different stages of the model profile. a) 1000 steps, b) 2000 steps, c) 3000 steps, d) 4000 steps.

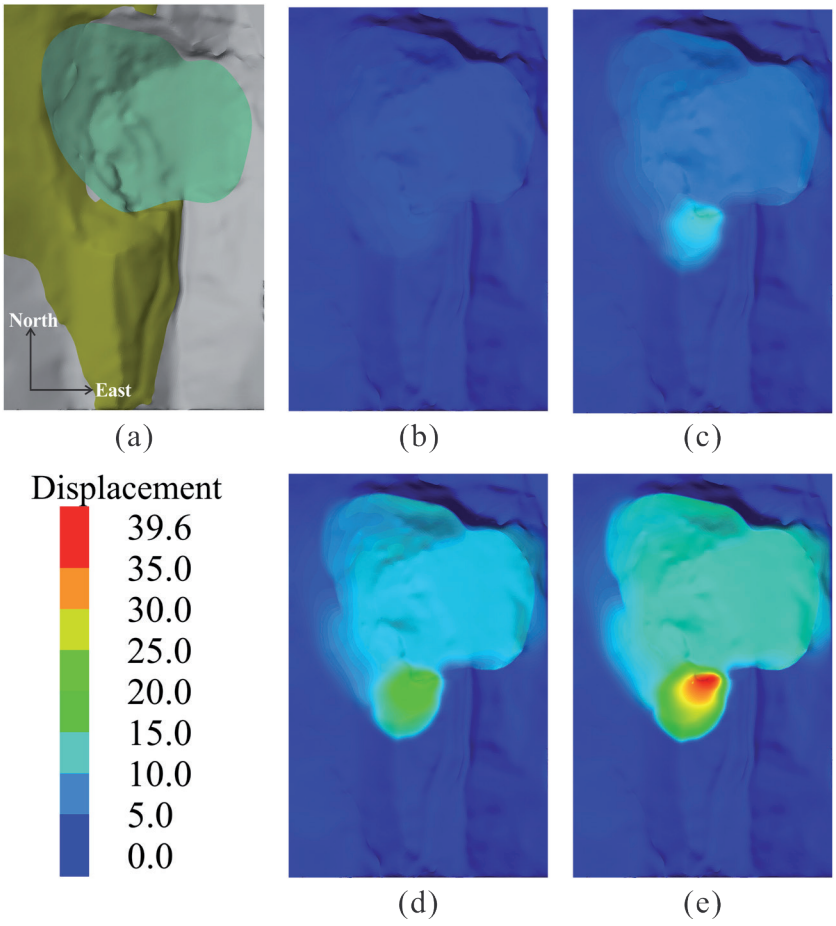

Fig. 8. Surface displacement cloud maps at different stages of the model. a) Numerical model, b) 1000 steps, c) 2000 steps, d) 3000 steps, e) 4000 steps.

shown in Fig. 3, it is observed that after 1,000 simulation steps, the stope roof in the mined-out area has undergone noticeable displacement. However, the upward transmission of this displacement to the ground surface remains limited, resulting in only minor surface subsidence. This finding suggests a lag effect between underground mining and surface subsidence. In the model, a constant subsidence rate was applied to the roof of the initial mining area to simulate ongoing collapse in the existing subsidence zone. According to the simulation results at 1,000 steps, the displacement at the top of the southern mining area is lower than that at the initial mining area, indicating that the subsidence rate in the southern mining area is lower than that in the initial mining area during the first 1,000 steps. However, from 2,000 steps onwards, the displacement at the top of the southern mining area exceeds that of the initial mining area, and the difference between the two increases progressively. Regarding spatial distribution, the surface subsidence induced by mining in the southern area exhibits an approximately circular pattern, with the most significant subsidence occurring along the northern edge.

Fig. 9 shows the vertical displacement (Z-direction) of the monitoring points in the simulation, with values ranging from 0 to 37 m. Except for monitoring points 18, 19, 20, and 21, which are not significantly affected by mining activities, the remaining monitoring points exhibit nonlinear increases in vertical displacement as the calculations progress, with an accelerating subsidence rate. Consistent with the displacement contour results, monitoring points 3 to 10, located in the northern part of the mined-out area, exhibit the most significant displacement and the fastest subsidence rates. An examination of displacement at monitoring points 4 to 17 reveals that, although all adjacent points are spaced only 10 m apart along the Y-direction, there are substantial differences in their final displacement values. A clear trend is observed: the southern monitoring points exhibit greater displacement differences and a more pronounced vertical displacement gradient.

Fig. 10 shows the simulated vertical displacement (Z-direction) of the monitoring line at various stages. After 1,000 simulation steps, the displacements are relatively small, and the differences in subsidence values between locations along the line are minimal. By 2,000 steps, the displacement of the monitoring points becomes more pronounced, with different locations exhibiting varying patterns of change. The segment between 50 m and 70 m, located at the boundary of the subsidence zone, experiences rapid subsidence, whereas the displacement along the line between 70 m and 170 m becomes more gradual. At 170 m, the maximum subsidence is observed, with a vertical displacement of up to 10 m. As the simulation progresses to 3,000 and 4,000 steps, subsidence increases further, and the displacement gradient along the monitoring line becomes even steeper. At 2,000 steps, the maximum displacement gradient occurs at the subsidence boundary (50-70 m), and this feature persists at 3,000 and 4,000 steps, with the affected segment length gradually increasing over time.

A field survey was conducted to investigate surface subsidence in the study area and delineate the subsidence

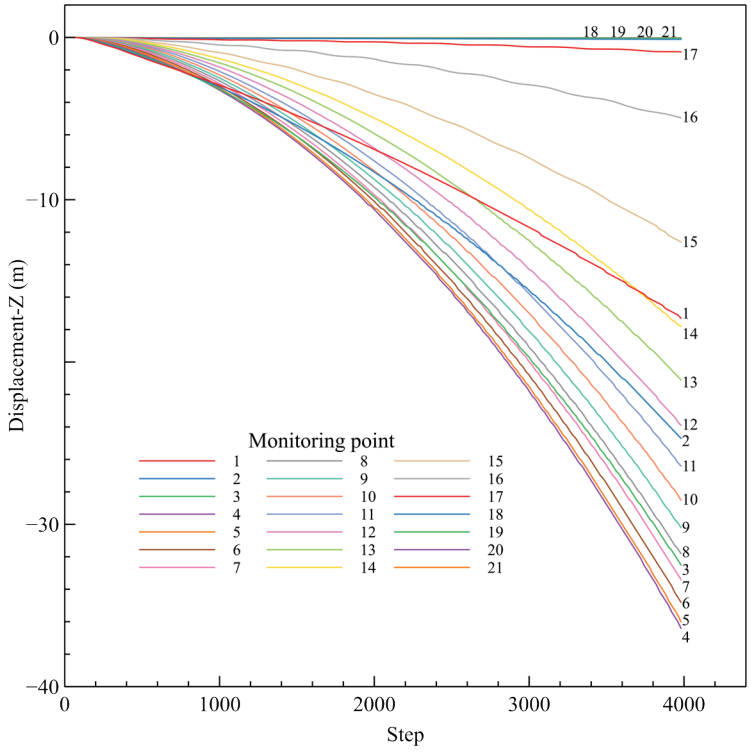

Fig. 9. Z-direction displacement curve of monitoring points in the numerical simulation.

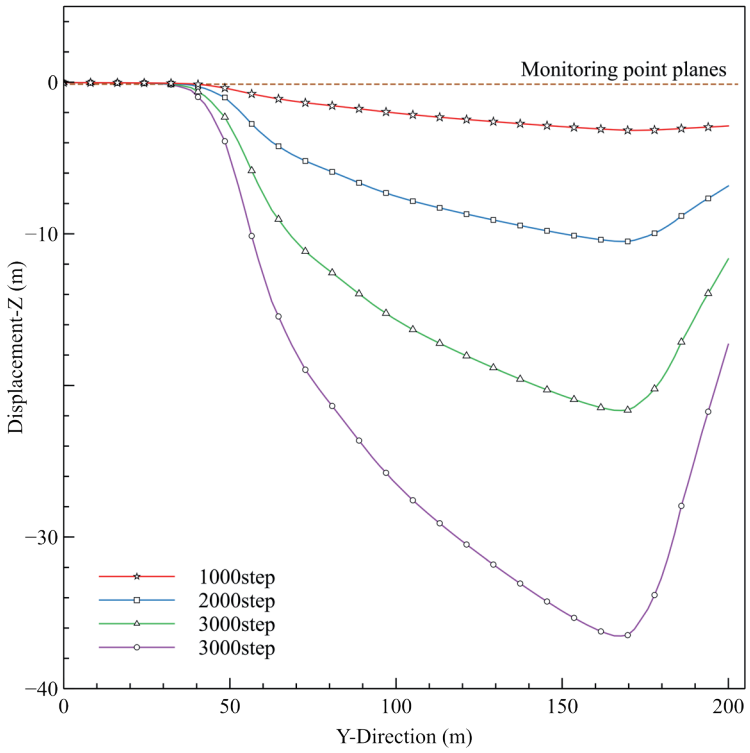

Fig. 10. Z-direction displacement curves at different stages along the straight line of monitoring points.

boundary as of May 2025, as shown in Fig. 11. In Fig. 11a), the red line indicates the subsidence boundary observed in the UAV orthophotography. Fig. 11b) shows the subsidence boundary superimposed on the digital model constructed from the contour map.

A comparison between the numerical simulation results at 4,000 steps and the actual subsidence boundary, as shown in Fig. 11b), is presented in Fig. 12. As observed from the simulation results, the simulated subsidence zone shows good agreement with the actual subsidence area, particularly regarding the southern subsidence region boundary, where the simulated and observed boundaries closely match. This consistency validates the numerical simulation approach. However,

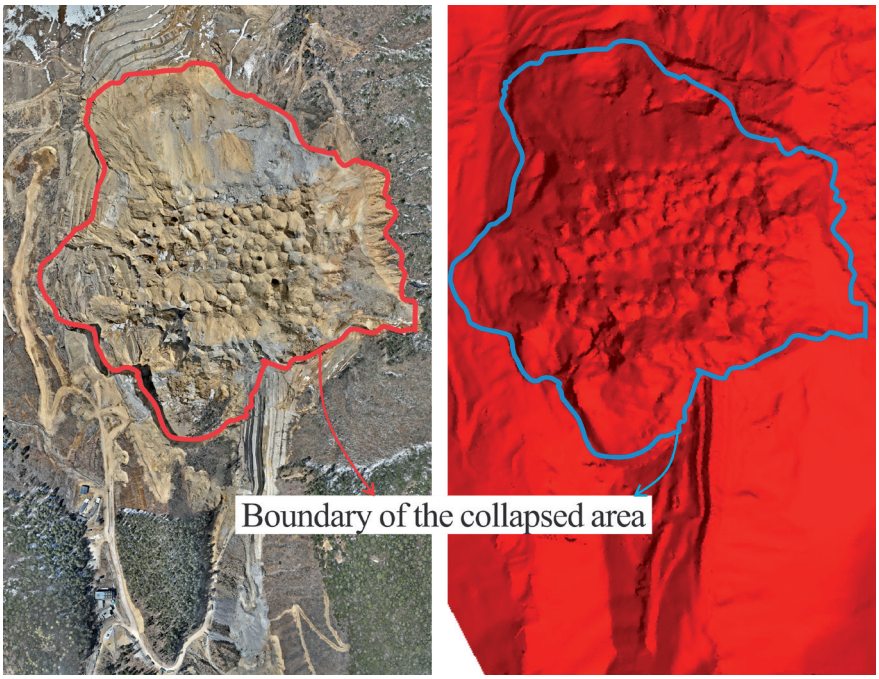

Fig. 11. Surface subsidence boundary (2025). a) Aerial view, b) numerical model.

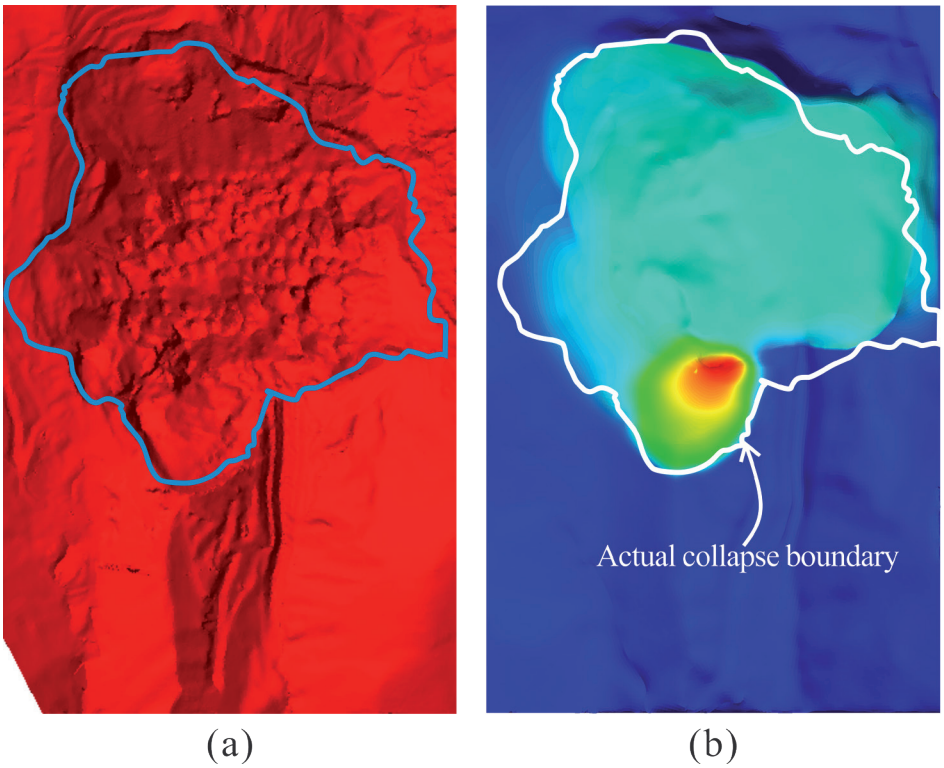

Fig. 12. Comparison of simulated results with actual subsidence results. a) Actual subsidence results, b) numerical simulation results.

since the simulation simplified the subsidence process in the initial mining area by applying a constant downward velocity at its base, some discrepancies remain between the simulated and actual subsidence results. For example, the simulation shows pronounced subsidence displacement in the north-eastern area, whereas the actual extent of subsidence in this region is more limited. This discrepancy may be attributed to a lower ore extraction volume in this area during actual mining operations. In addition, the eastern part of the southern mining area shows slight displacement in the simulation, despite being within the actual subsidence boundary. Overall, although underground mining zones are constrained within a specified area, the ore extraction process is highly complex and uneven across regions, leading to discrepancies between simulated and observed subsidence. Nevertheless, a comparative analysis demonstrates that the simulation results remain highly informative and serve as a valuable reference.

Prediction Study of Surface Subsidence Induced by Underground Mining

Predicting surface subsidence zones caused by underground mining is crucial for engineering construction and for the safety of life and property in mining areas. Effective monitoring and control of potential hazard zones can help mitigate subsidence-related losses. The previous results show that the subsidence boundaries predicted by numerical simulations agree with the actual subsidence boundaries. In this chapter, numerical simulations are conducted to predict changes in surface subsidence caused by mining activities in a newly developed underground area. Specifically, a new mining zone is designed in the southern part of the mining district, as shown in Fig. 13, where the red area represents the proposed new mining area.

Numerical simulations were conducted for the new mining scenario, and the resulting surface displacement is shown in Fig. 14. The simulation results are similar to those obtained for the southern mining area in Fig. 8. As the simulation progresses, the subsidence displacement above the mining area increases, and the subsidence zone gradually extends southward. The subsidence displacement exhibits a pronounced gradient across locations, with a displacement of 40 m in the core subsidence area after 4,000 simulation steps.

Based on the numerical simulation results shown in Fig. 14, the subsidence zone boundary was delineated and compared with the actual subsidence boundary. The combined boundaries are overlaid on the map of the actual subsidence area, as shown in Fig. 15. The boundary extends southward at this stage, with the southernmost Y-coordinate reaching 3.10267×10^{6}. Subsidence has now affected most of the southern drainage ditch project, posing a significant risk of failure to the drainage infrastructure and warranting heightened attention. Additionally, the expansion of the subsidence area alters surface topography, potentially triggering geological hazards such as landslides and debris flows.

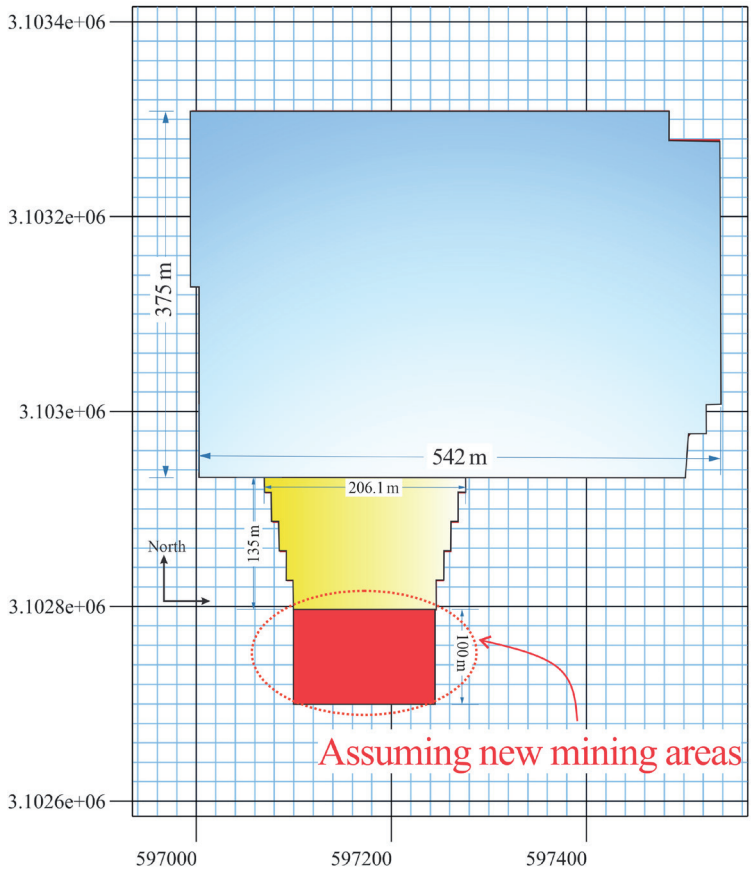

Fig. 13. Designated range of the new mining area.

Discussion

The numerical simulation results obtained in this study reveal the progressive transmission of deformation from underground mined-out areas to the surface, ultimately forming a stable subsidence boundary that agrees well with the measured data. This finding is broadly consistent with the research of Parmar et al. [27] on deformation propagation in underground metal mines, which similarly reported that hanging-wall movement dominates the upward transfer of rock mass deformation. Compared with those studies, however, the present work provides a more detailed three-dimensional characterization of the collapse geometry in a complex porphyry copper deposit, demonstrating the capability of FLAC^{3D} to reproduce large-scale natural collapse phenomena.

In addition, the observed trend of continuous increase in vertical displacement within the collapse zone, coupled with stabilization of the overall subsidence boundary, aligns with the staged development pattern of mining-induced sinkholes described by Li et al. [32], who identify phases of rapid local deformation followed by a plateau in boundary expansion once critical failure surfaces have formed. These studies show that although local deformation may continue to accumulate, the macro-scale geometry of the subsidence basin often reaches a quasi-steady configuration, suggesting a self-limiting mechanism controlled by the formation of stable failure surfaces. The present simulations further support this conceptual model by providing a dynamic visualization of boundary evolution across multiple excavation steps, illustrating how incremental mining stages drive internal subsidence while the external boundary matures and stabilizes.

Nevertheless, discrepancies between the simulated and measured boundaries in certain areas highlight the limitations of the current modelling approach, similar to inconsistencies documented in numerical studies of hard-rock collapse zones by Zhao et al. [33], who attribute divergence between model predictions and field observations to spatially heterogeneous excavation sequences, unmodeled engineering activities (such as localized supports or backfilling), and time-dependent mechanical behavior, including damage accumulation and delayed failure. In our case, the nonuniformity of the actual mining sequence, along with post-collapse mitigation measures (e.g., partial backfilling, reinforcements), likely had a significant effect on surface deformation that was not explicitly incorporated into our model. Furthermore, uncertainties in parameterization – such as in situ stress, rock mass strength, and joint network geometry – may exacerbate mismatches. These limitations suggest that future simulations would benefit significantly from incorporating more detailed, site-specific operational data and realistic excavation histories.

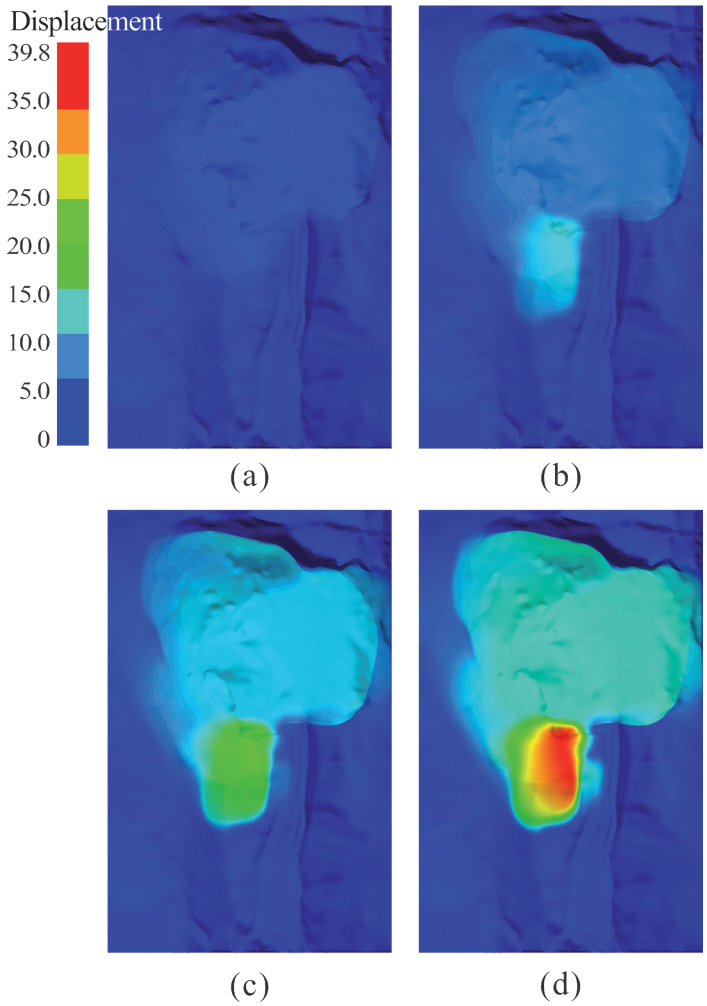

Fig. 14. Surface displacement cloud maps of the designed mining activity. a) 1000 steps, b) 2000 steps, c) 3000 steps, d) 4000 steps.

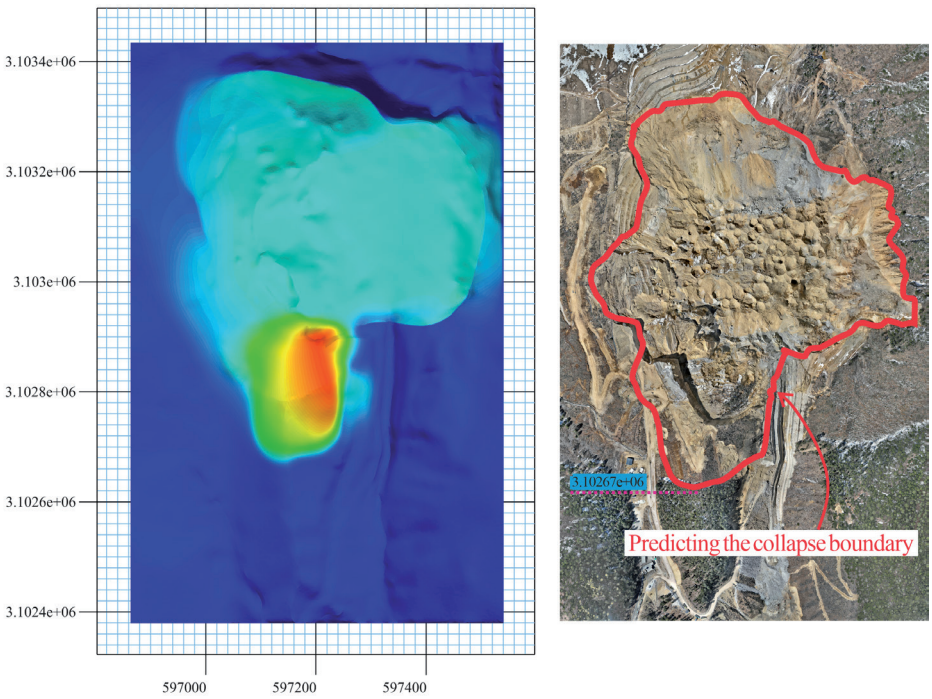

Fig. 15. Subsidence boundary caused by the designed mining activity. a) Displacement cloud map at 4000 steps, b) subsidence boundary location.

Moreover, this study focused solely on mining-induced subsidence and did not account for the combined effects of engineering interventions, hydrological evolution, or long-term creep, as in studies such as Zhang et al. [34] and Liang et al. [35] have shown to be significant contributors to surface deformation in deep mining districts.

In this context, integrating multi-physical processes such as creep deformation, groundwater flow, hydro-mechanical coupling, and engineered mitigation (e.g., backfill, structural support) represents a critical direction for future modelling. Incorporating such aspects could lead to more realistic simulations of boundary evolution, more accurate forecasts of long-term subsidence, and improved risk assessments. For example, future work might calibrate models using long-term monitoring data (InSAR, GPS, microseismicity) to constrain parameterizations of creep and water-rock interaction; better representation of excavation and support histories could improve the fidelity of predicted boundary behavior over time.

Overall, the present findings contribute to the growing body of knowledge on natural collapse mining and surface subsidence. By providing a validated 3D geological modelling workflow, this work offers a valuable reference for similar underground mining projects. Future research should aim to integrate high-resolution monitoring, machine-learning-based data fusion, and calibrated excavation schedules to overcome the current limitations and enhance early-warning and prediction capabilities.

Conclusions

In this study, based on the actual engineering conditions of the Pulang Copper Mine, a numerical simulation approach was systematically employed to analyse surface subsidence phenomena induced by sublevel caving mining methods. Based on this, the potential surface subsidence caused by subsequent mining activities was predicted, providing crucial scientific support for production activities and disaster prevention in the mining area.

The numerical simulation results indicate that areas adjacent to the initial mining zone, where the surrounding rock offers weaker lateral support, are the first to experience significant subsidence. Moreover, the displacement caused by the collapse of the underground ore body is gradually transmitted upward, resulting in a pronounced lag effect in surface subsidence. With ongoing mining activities, subsidence continues to expand, and the subsidence rate in specific regions increases markedly. Overall, the simulation results agree with the field-measured surface subsidence, particularly in the southern mining area, where the method demonstrates high predictive accuracy and practical utility for future mining-induced subsidence trends.

Further numerical predictions indicate that, under the new mining conditions, continued extraction in the southern mining area will result in additional expansion of the subsidence zone, potentially causing severe impacts on existing infrastructure, such as drainage ditches. These findings provide a critical basis for future engineering planning and formulating disaster prevention measures in the mining area.

This study proposes an effective numerical simulation method for addressing surface subsidence problems associated with mining operations. The technique provides a scientific basis for safety management, engineering optimization, and environmental protection in mining areas, offering solid technical support for risk assessment and mitigation measures during mining activities.

Acknowledgments

Funding: This work was supported by The National Key Science and Technology Project for Deep Earth (No.: 2024ZD1001400).

Conflict of Interest

The authors declare no conflict of interest.

References

1. BLODGETT S., KUIPERS J.R. Underground Hard-Rock Mining: Subsidence and Hydrologic Environmental Impacts. ResearchGate, **2002**.
2. LUO Y., CHENG J. An influence function method based subsidence prediction program for longwall mining operations in inclined coal seams. Mining Science and Technology (China), **19** (5), 592, **2009**.
3. HUAYANG D., XUGANG L., JIYAN L., YIXIN L., YAMENG Z., WEINAN D., YINFEI C. Model study of deformation induced by fully mechanized caving below a thick loess layer. International Journal of Rock Mechanics and Mining Sciences, **47**, 1027, **2010**.
4. WANG B., XU J., XUAN D. Time function model of dynamic surface subsidence assessment of grout-injected overburden of a coal mine. International Journal of Rock Mechanics and Mining Sciences, **104**, 1, **2018**.
5. YAN W., CHEN J., YAN Y. A new model for predicting surface mining subsidence: the improved lognormal function model. Geosciences Journal, **23** (1), 165, **2019**.
6. ZHANG L., CHENG H., YAO Z., WANG X. Application of the Improved Knothe Time Function Model in the Prediction of Ground Mining Subsidence: A Case Study from Heze City, Shandong Province, China. Applied Sciences, **10** (9), 3147, **2020**.
7. NASIRI A., SHAFIEE N., ZANDI R. Spatial analysis of factors influencing land subsidence using the OLS Model (Case Study: Fahlian Aquifer). Earth Science Informatics, **14** (4), 2133, **2021**.

8. LI H., ZHU L., GUO G., ZHANG Y., DAI Z., LI X., CHANG L., TEATINI P. Land subsidence due to groundwater pumping: hazard probability assessment through the combination of Bayesian model and fuzzy set theory. Natural Hazards and Earth System Sciences, **21** (2), 823, **2021**.
9. ROSA A.G.F., SILVA W.D.O., FONTANA M.E., LEVINO N., GUARNIERI P. A GIS-based multi-criteria approach for identifying areas vulnerable to subsidence in the world's largest ongoing urban socio-environmental mining disaster. The Extractive Industries and Society, **19**, 101500, **2024**.
10. GUÉGUEN Y., DEFFONTAINES B., FRUNEAU B., AL HEIB M., DE MICHELE M., RAUCOULES D., GUISE Y., PLANCHENAULT J. Monitoring residual mining subsidence of Nord/Pas-de-Calais coal basin from differential and Persistent Scatterer Interferometry (Northern France). Journal of Applied Geophysics, **69** (1), 24, **2009**.
11. ZHAO H., MA F., ZHANG Y., GUO J. Monitoring and mechanisms of ground deformation and ground fissures induced by cut-and-fill mining in the Jinchuan Mine 2, China. Environmental Earth Sciences, **68** (7), 1903, **2013**.
12. XIA K., CHEN C., DENG Y., XIAO G., ZHENG Y., LIU X., FU H., SONG X., CHEN L. In situ monitoring and analysis of the mining-induced deep ground movement in a metal mine. International Journal of Rock Mechanics and Mining Sciences, **109**, 32, **2018**.
13. GONG H., PAN Y., ZHENG L., LI X., ZHU L., ZHANG C., HUANG Z., LI Z., WANG H., ZHOU C. Long-term groundwater storage changes and land subsidence development in the North China Plain (1971–2015). Hydrogeology Journal, **26** (5), 1417, **2018**.
14. WEMPEN J.M. Application of DInSAR for short period monitoring of initial subsidence due to longwall mining in the mountain west United States. International Journal of Mining Science and Technology, **30** (1), 33, **2020**.
15. MA X., FU Z., LI Y., ZHANG P., ZHAO Y., MA G. Study on Surface Subsidence Characteristics Based on Three-Dimensional Test Device for Simulating Rock Strata and Surface Movement. Energies, **15** (5), 1927, **2022**.
16. PENG M., LU Z., ZHAO C., MOTAGH M., BAI L., CONWAY B.D., CHEN H. Mapping land subsidence and aquifer system properties of the Willcox Basin, Arizona, from InSAR observations and independent component analysis. Remote Sensing of Environment, **271**, 112894, **2022**.
17. MUHETAER N., YU J., WANG Y., YUE J. Temporal and Spatial Evolution Characteristics Analysis of Beijing Land Subsidence Based on InSAR. IOP Conference Series: Earth and Environmental Science, **658** (1), 012050, **2021**.
18. MA B., GAO R., CHE D., XU Z., WANG D., SUN Y. Multisource remote sensing monitoring and analyzing for land subsidence and crop growth in a coal mining area under different rainfall conditions. Environmental Development, **52**, 101086, **2024**.
19. MANCINI F., STECCHI F., GABBIANELLI G. GIS-based assessment of risk due to salt mining activities at Tuzla (Bosnia and Herzegovina). Engineering Geology, **109** (3), 170, **2009**.
20. HELM P.R., DAVIE C.T., GLENDINNING S. Numerical modelling of shallow abandoned mine working subsidence affecting transport infrastructure. Engineering Geology, **154**, 6, **2013**.
21. HUANG G., KULATILAKE P.H.S.W., SHREEDHARAN S., CAI S., SONG H. 3-D discontinuum numerical modeling of subsidence incorporating ore extraction and backfilling operations in an underground iron mine in China. International Journal of Mining Science and Technology, **27** (2), 191, **2017**.
22. FATHI SALMI E., NAZEM M., KARAKUS M. Numerical analysis of a large landslide induced by coal mining subsidence. Engineering Geology, **217**, 141, **2017**.
23. HAMDI P., STEAD D., ELMO D., TÖYRÄ J. Use of an integrated finite/discrete element method-discrete fracture network approach to characterize surface subsidence associated with sub-level caving. International Journal of Rock Mechanics and Mining Sciences, **103**, 55, **2018**.
24. WU G., JIA S., WU B., YANG D. A discussion on analytical and numerical modelling of the land subsidence induced by coal seam gas extraction. Environmental Earth Sciences, **77** (9), 353, **2018**.
25. LIU X.-J., CHENG Z.-B. Changes in subsidence-field surface movement in shallow-seam coal mining. Journal of the Southern African Institute of Mining and Metallurgy, **119**, 12, **2019**.
26. CHEN D., CHEN H., ZHANG W., CAO C., ZHU K., YUAN X., DU Y. Characteristics of the Residual Surface Deformation of Multiple Abandoned Mined-Out Areas Based on a Field Investigation and SBAS-InSAR: A Case Study in Jilin, China. Remote Sensing, **12** (22), 3752, **2020**.
27. PARMAR H., BAFGHI A.Y., NAJAFI M. Impact of ground surface subsidence due to underground mining on surface infrastructure: the case of the Anomaly No. 12 Sechahun, Iran. Environmental Earth Sciences, **78** (14), 409, **2019**.
28. ZHAO X., YU W., ZHAO Y., FU S. Numerical Estimation of Shaft Stability and Surface Deformation Induced by Underground Mining Transferred from Open-Pit Mining in Jinfeng Gold Mine. Minerals, **13** (2), 196, **2023**.
29. CAI W., LI L., LIN M., WANG J., WANG P., LI Q., YE Z., ZHANG J., ZHAO J. Prediction of surface deformation induced by mining thin coal seam: A case study of Guanshan coalfield in Sichuan. Natural Hazards Research, **4** (2), 255, **2024**.
30. ZHOU S., WANG H., SHAN C., LIU H., LI Y., LI G., YANG F., KANG H., XIE G. Dynamic Monitoring and Analysis of Mining Land Subsidence in Multiple Coal Seams in the Ehuobulake Coal Mine Based on FLAC3D and SBAS-InSAR Technology. Applied Sciences, **13** (15), 8804, **2023**.
31. GONG Y.-Q., GUO G.-L., WANG L.-P., LI H.-Z., ZHANG G.-X., FANG Z. A Data-Intensive Numerical Modeling Method for Large-Scale Rock Strata and Its Application in Mining Subsidence Prediction. Rock Mechanics and Rock Engineering, **55** (3), 1687, **2022**.
32. LI G., WAN Y., GUO J., MA F., ZHAO H., LI Z. A Case Study on Ground Subsidence and Backfill Deformation Induced by Multi-Stage Filling Mining in a Steeply Inclined Ore Body. Remote Sensing, **14** (18), 4555, **2022**.
33. ZHAO Y., ZHAO X., DAI J., YU W. Analysis of the Surface Subsidence Induced by Mining Near-Surface Thick Lead-Zinc Deposit Based on Numerical Simulation. Processes, **9** (4), 717, **2021**.
34. ZHANG H., GUO G., LI H., WANG T., NI J., MENG H. A new numerical method for calculating residual deformation in mined-out areas considering water–rock interaction and its application. Scientific Reports, **15** (1), 11207, **2025**.

35. LIANG Z., YANG X., LIU Y., ZHANG B. A prediction method for long-term surface subsidence considering the mining-induced stratum creep effect and its application. Scientific Reports, **15** (1), 38968, **2025**.